Molecular Therapy
Nucleic Acids
Original Article

MicroRNA-29b Mediates Lung Mesenchymal-Epithelial Transition and Prevents Lung Fibrosis in the Silicosis Model

Jingping Sun,[1,2] Qiuyue Li,[1,2] Ximeng Lian,[1,2] Zhonghui Zhu,[1,2] Xiaowei Chen,[1,2] Wanying Pei,[1,2] Siling Li,[1,2] Ali Abbas,[1,2] Yan Wang,[1,2] and Lin Tian[1,2]

[1]Department of Occupational Health and Environmental Health, School of Public Health, Capital Medical University, Beijing 100069, China; [2]Beijing Key Laboratory of Environmental Toxicology, Capital Medical University, Beijing 100069, China

Lung epithelial-mesenchymal transition (EMT) plays an important role in silicosis fibrosis. The reverse process of EMT is mesenchymal-epithelial transition (MET), which is viewed as an anti-EMT therapy and is a good target toward fibrosis. MicroRNAs (miRNAs) have emerged as potent regulators of EMT and MET programs, and, hence, we tested the miRNA expression using microarray assay and investigated their roles in silica-induced EMT in lung epithelial cells. We found that miRNA-29b (miR-29b) was dynamically downregulated by silica and influenced the promotion of MET in RLE-6TN cells. Furthermore, delivery of miR-29b to mice significantly inhibited silica-induced EMT, prevented lung fibrosis, and improved lung function. Together, our results clearly demonstrated that miR-29b acted as a novel negative regulator of silicosis fibrosis-inhibited lung fibrosis, probably by promoting MET and by suppressing EMT in the lung. These findings may represent a new potential therapeutic target for treating silicosis fibrosis.

INTRODUCTION

Silicosis is an occupational disease that is caused by inhalation of crystalline silica and is characterized by silicotic nodules and lung fibrosis. The pathogenesis of silicosis involves an initial immune response, followed by injury to the alveolar cells, expansion and activation of fibroblasts, and, ultimately, the deposition of the extracellular matrix (ECM). Despite the long-standing and continuing efforts from the World Health Organization and many countries to try to eliminate silicosis, many new clinical cases relating to silicosis fibrosis continue to emerge,[1] especially in developing countries. Currently, there is no effective therapy to delay the progress of silicosis, which can progress after exposure to silica has ceased.[2] For this reason, it is necessary to investigate the complex molecular mechanisms that underlie the disease.

The proliferation and accumulation of fibroblasts are considered to be vital in the development of pulmonary fibrosis diseases.[3] A large proportion of data implicates that epithelial cells undergoing the process of epithelial-mesenchymal transition (EMT) is one source of fibroblasts.[4,5] During EMT, epithelial cells gradually lose their epithelial characteristics and transform into a mesenchymal-like cell phenotype, which begins to synthesize the components of ECM, such as collagen I and fibronectin. Among the extracellular cytokines that activate EMT, transforming growth factor β (TGF-β) is known to be the main inducer. The TGF-β-signaling pathway is most likely to be the best-characterized pathway that can activate key regulators like Snail to subsequently trigger EMT.[6] Our previous study revealed that EMT and the activating TGF-β pathway were closely associated with silicosis fibrosis.[7,8] The reverse process of EMT is mesenchymal-epithelial transition (MET), in which epithelial characteristics are re-acquired.[9] MET is viewed as an anti-EMT therapy and a good target for treating fibrosis. The mechanisms underlying MET and EMT are complicated due to the fact that many transcription factors and signaling pathways can initiate them.[10] Recent research shows that microRNAs (miRNAs) act as important regulators of MET and EMT programs by targeting the key proteins that regulate these processes.[11]

miRNAs are short (22-nt), non-coding, and single-stranded RNAs. They function by suppressing each target through complementary binding to the 3′ UTR of the target gene, resulting in mRNA degradation and translational repression. Several studies have identified that miRNAs are involved in pulmonary fibrosis. Furthermore, studies have shown that the initial injury of epithelial cells initiates upregulation of pro-fibrotic miRNAs and downregulation of anti-fibrotic miRNAs, which regulate EMT and MET in epithelial cells. The previous research has found that reducing the miR-200 family resulted in increased levels of ZEB1/2 and promoted the EMT progression, while

Received 11 May 2018; accepted 31 October 2018;
https://doi.org/10.1016/j.omtn.2018.10.017.

Correspondence: Lin Tian, Department of Occupational Health and Environmental Health, School of Public Health, Capital Medical University, No. 10, Xi toutiao outside You anmen Street, Beijing 100069, China.
E-mail: tian_lin@163.com
Correspondence: Yan Wang, Department of Occupational Health and Environmental Health, School of Public Health, Capital Medical University, No. 10, Xi toutiao outside You anmen Street, Beijing 100069, China.
E-mail: wangyan6464@sina.com

an upregulation of miR-200 inhibited EMT or enhanced MET.[12] Some scholars observed that let-7d was downregulated in TGF-β-induced EMT in lung epithelial cells and the downregulation of let-7d caused EMT in the lungs of mice.[13] Although these miRNAs' exact roles in EMT or MET remain to be explored, several miRNA-targeted therapies have reached clinical developments. An example of such a miRNA-targeted therapy is miR-200 mimics, which provide an attractive therapeutic strategy for diabetes.[14] The ability of miRNAs to target multiple mRNAs altered in diseases makes these miRNAs candidates as therapeutics potential or suggests their use as targets of therapeutics. For this reason, we explored the miRNA alteration in silicosis fibrosis and intended to find a candidate miRNA.

Here we performed a large-scale screen for miRNAs potentially involved in silicosis fibrosis. Using the silica-induced EMT model *in vitro*, we revealed that miRNA-29b (miR-29b) was among those most significantly reduced miRNAs. This reduction *in vitro* and *in vivo* correlated with EMT progression and increased expression of ECM-related genes. Moreover, we found that upregulation of miR-29b promoted MET, prevented EMT, and inhibited the expression of ECM-related genes. Meanwhile, downregulation of miR-29b enhanced EMT and upregulated ECM-related genes. Together, our study supports a role for miR-29b in the pathogenesis of silicosis fibrosis, and it suggests that miR-29b may be a candidate therapeutic target in silicosis.

RESULTS

Silica Induced an EMT Profile and Downregulated miR-29b Expression in AEII Cell Lines

We have previously shown that silica induced EMT *in vivo* and *in vitro*,[15,16] and we re-verified the EMT model induced by silica in A549 cells (a type of AEII cell line). The cells were treated with increasing concentrations of silica, ranging from 25 to 100 μg/mL. The MTT ((4, 5-dimethyl-2-thiazolyl)-2, 5-diphenyl-2-H-tetrazolium bromide) assay indicated that the viability of A549 cells was reduced with the increasing doses of silica, and 50 μg/mL silica showed the highest cytotoxicity at 48 hr (Figure 1A). Furthermore, we tested the expression of the mesenchymal marker (vimentin) and the most important transcriptional factor of EMT (Snail) using western blot. Silica exposure resulted in the increased expression of vimentin and Snail (Figure 1B) in a dose-dependent manner, peaking at 50 μg/mL. We also assessed the expression of EMT markers using immunofluorescence staining. The analysis confirmed the above results of vimentin. It showed that the levels of vimentin increased in cytoplasm with the increasing doses of silica and reached the highest at 50 μg/mL. The expression of the epithelial marker E-cadherin was observed mainly in the cell membrane in the control group, but after the addition of silica it was downregulated with the increase of silica and mainly expressed in the cytoplasm (Figure 1C). Silica also promoted the migration of A549 cells, which is shown in Figure 1D. The data suggested that 50 μg/mL silica induced an EMT profile in A549 cells.

Recent studies have shown that miRNA is very important in EMT and fibrosis diseases.[17,18] Thus, miRNA microarray was performed in silica-induced EMT. Based on preliminary studies, we used 50 μg/mL silica to induce EMT in the silica group. As shown in Figure 1E, in the silica group, silica infusion resulted in a significant downregulation of miR-200c, miR-149, and miR-29b. We have previously demonstrated that miR-29b displayed anti-fibrotic functions, downregulating collagen expression in silica-treated lung fibroblast cells,[19] but the exact role of miR-29b in epithelial cells was not clear, so we focused on silica-downregulated expression of miR-29b. It was further confirmed by qPCR (Figure 1F).

To confirm the vital functions of miR-29b in epithelial cells, we verified the above results in RLE-6TN cells, another type of AEII cell line. Exposure of RLE-6TN cells to silica for 48 hr also resulted in EMT and a decrease in miR-29b gene expression (Figure 2). The morphology of RLE-6TN cells changed from a typical epithelium to the mesenchymal spindle morphology (Figure 2A; Figure S1). Western blot revealed that silica induced the downregulation of E-cadherin and the upregulation of vimentin (Figure 2B). qPCR analysis showed the mRNA expression of E-cadherin (CDH1) was significantly reduced ($p < 0.01$), whereas vimentin and α-SMA dramatically increased in the silica group ($p < 0.01$) (Figure 2C). Meanwhile, the expression of miR-29b was downregulated obviously in the silica group (Figure 2D).

Above all, the results revealed that silica induced EMT and a downregulation of miR-29b expression in AEII cell lines.

miR-29b Mimics Promoted MET and Reversed EMT in RLE-6TN Cells

Cushing et al.[20] attributed the upregulation of pro-fibrotic genes to the downregulation of miR-29. However, the role of miR-29b in EMT and MET was not fully illustrated. To investigate whether miR-29b was able to reverse EMT and induce MET, we delayed the transfection of miR-29b mimics until EMT was established, and then we analyzed the levels of E-cadherin, vimentin, and α-SMA genes as well as the protein expressions of E-cadherin and vimentin in RLE-6TN cells. We first examined the efficiency of transfection by fluorescently labeled miR-29b mimics (Figure 3A). The transfection of miR-29b mimics markedly increased miR-29b levels (Figure 3A). miR-29b mimics induced the upregulation of CDH1 expression and downregulation of the expression of VIM (vimentin gene) and α-SMA (Figure 3B). Snail, one of the most important transcriptional repressors of E-cadherin, was upregulated by silica in our previous study.[8] Interestingly, the gene of Snail (snai1) was not altered after the addition of miR-29b mimics (Figure 3C). The protein ratio of E-cadherin:vimentin was also evaluated, as it was found to correlate significantly with EMT status. The analysis showed that the ratio was elevated in the silica + miR-29b mimic group compared with the silica + negative control (NC) group (Figure 3D), suggesting that miR-29b promoted MET and inhibited EMT.

Moreover, we were able to confirm these results with the classical EMT model (Figures 3E–3H), in which TGF-β1 was used to replace

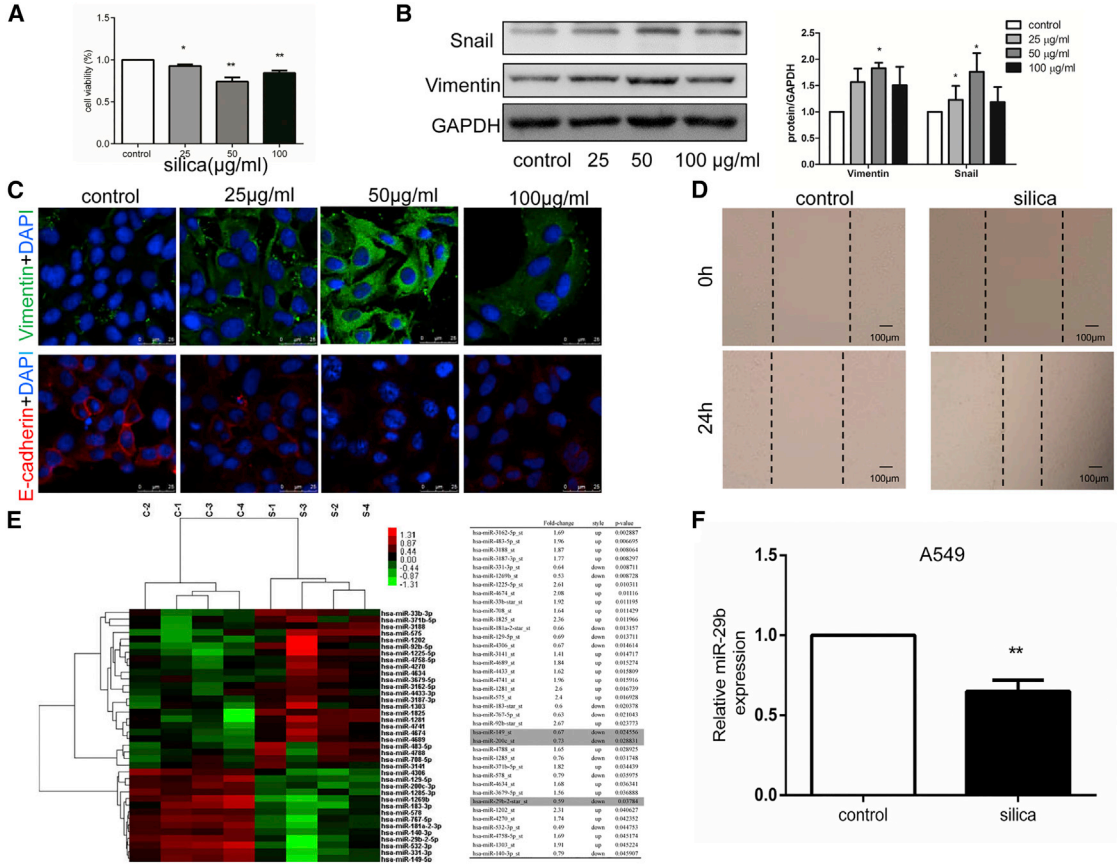

Figure 1. Silica Induced EMT and Alterations of miRNA Expression in A549 Cells

(A) Cytotoxicity of silica in A549 cells. The cells were treated with different concentrations of silica (25, 50, and 100 μg/mL). Cell viability was defined as 100% when cells were cultured with DMEM only. (B) Western blot analyses revealed that the protein expression of vimentin and Snail was upregulated gradually along with increased levels of silica in A549 cells. (C) Immunofluorescence staining for E-cadherin (red) and vimentin (green) confirmed that silica induced EMT in A549 cells. (D) The wound-healing assay showed that silica induced migration of A549 cells. (E) miRNA microarray showed that the expressions of miR-200c, miR-149, and miR-29b were significantly downregulated in A549 cells treated with 50 μg/mL silica. (F) The results of qPCR confirmed that the level of miR-29b was significantly decreased in A549 cells. All results were replicated at least three times independently. The data are presented as means ± SD. $*p < 0.05$ and $**p < 0.01$ versus the control group.

silica treatment. Based on previously published studies, we used 5 ng/mL TGF-β1 to induce EMT in RLE-6TN cells. As shown in Figure 3E, after TGF-β1 treatment for 48 hr, downregulation of CDH1 was accompanied by an upregulation of α-SMA and COL1A1 (collagen I gene) (Figure 3E). TGF-β1 also decreased the level of miR-29b (Figure 3F). However, miR-29b mimics significantly suppressed the expression of VIM, α-SMA, COL1A1, and Tgfb1 (TGF-β1 gene) (Figure 3G) and elevated the protein ratio of E-cadherin:vimentin (Figure 3H). It showed that miR-29b mimics promoted MET and reversed EMT in RLE-6TN cells.

miR-29b Inhibitor Led to the Development of EMT in RLE-6TN Cells

To comprehensively illustrate the mechanism of miR-29b, we established cells that suppressed miR-29b by transiently transfecting with the miR-29b inhibitor (Figure 4A). The downregulation of miR-29b increased the levels of COL1A1 and snai1, induced by silica (Figures 4B and 4C). Furthermore, compared with the silica + inhibitor NC group, the protein ratio of E-cadherin:vimentin declined in the silica + miR-29b inhibitor group (Figure 4D), indicating the development of EMT. It suggested that the increase of Snai1 after the knockdown of miR-29b was associated with the enhanced EMT by miR-29b inhibitor.

In the TGF-β1-induced EMT model, the downregulation of miR-29b resulted in an increase in VIM, α-SMA, and COL1A1, whereas CDH1 dramatically decreased (Figure 4E). The effect of miR-29b inhibitor on the ratio of E-cadherin:vimentin showed to be similar to the silica-induced EMT model (Figure 4F). It showed that miR-29b inhibitor led to the development of EMT in RLE-6TN cells.

miR-29b Inhibits EMT and Pulmonary Fibrosis, Resulting in Lung Function Improvement in a Mouse Model of Silicosis Fibrosis

We subsequently decided to confirm whether miR-29b has a therapeutic effect in a mouse model of silicosis fibrosis. To investigate the effects

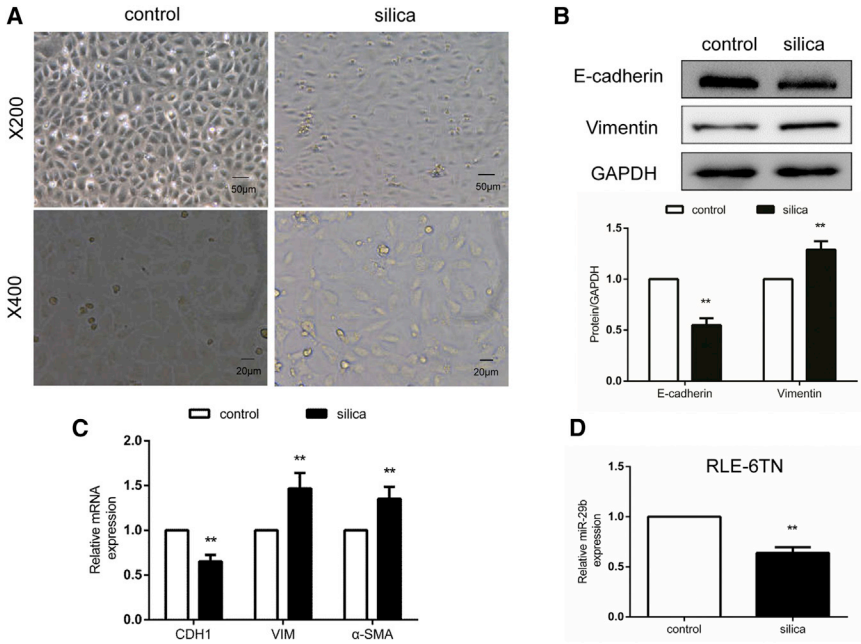

Figure 2. Silica (50 μg/mL) Induced EMT and the Downregulation of miR-29b in RLE-6TN Cells

(A) The RLE-6TN cells showed a typical epithelial cuboidal shape in the control group and spindle-shaped morphology in the silica group. (B) Western blot analyses showed that, in the silica group, the protein expression of E-cadherin was downregulated and vimentin expression was upregulated. (C) The results of qPCR revealed that silica obviously decreased the level of CDH1 and increased the levels of VIM and α-SMA. (D) The results of qPCR verified that the level of miR-29b was decreased in the silica group. All results were replicated at least three times independently. The data are presented as means ± SD. $^{*}p < 0.05$ and $^{**}p < 0.01$ versus the control group.

of miR-29b *in vivo*, mice were administered agomir-29b, which was far more stable *in vivo* than miRNA mimics. The dose did not produce any signs of discomfort in the mice. The mice in the control and silica groups were injected with an equal volume of saline, while silica + NC mice were administered with agomir NC at a dose of 5 nmol. The mice were sacrificed on the 28th day. By real-time PCR analysis, we detected that silica largely decreased miR-29b in the lung after silica instillation for 28 days. In contrast, the mice injected with the agomir-29b exhibited an obvious increase of miR-29b in the lungs (Figure 5B). We also detected the expression of miR-29b in the lungs by fluorescence *in situ* hybridization (FISH). The assay showed that silica decreased the level of miR-29b but agomir-29b significantly upregulated the expression of miR-29b in the cell nucleus (Figure 5C). These results revealed that agomir-29b upregulated the expression of miR-29b in the lungs of mice instilled with silica.

Next, we examined the preventive role of miR-29b on EMT, pulmonary fibrosis, and functional injury in response to the silica. Silica induced an evident EMT at day 28, as shown by the decrease of CDH1, whereas it increased the VIM and α-SMA. With that said, *in vitro*, upregulation of miR-29b blocked silica-induced EMT by restoring CDH1, whereas it clearly inhibited the expression of VIM and α-SMA (Figure 6A). In parallel to the *in vitro* study, upregulation of miR-29b did not affect the level of Snai1 (Figure 6B). Immunofluorescence confirmed the above-mentioned results at the protein level. The alveolar epithelial cells (arrows) in the lungs of the silica and silica + NC groups stained positive (green) for vimentin, whereas agomir-29b-treated mice did not express clear positive staining (Figures 6C and 6D).

H&E and Masson staining revealed that there were thickened alveolar septa, increased numbers of cell nodules, as well as areas of blue staining, which indicated the presence of collagen in the mice instilled with silica receiving no treatment or agomir NC, while agomir-29b decreased lung fibrosis significantly, as evidenced by the thickness of the alveolar septum, the decreased number of cell nodules, and the area of the blue fibers (Figure 7A). Similarly, the areas of the blue stain were calculated; it showed a significant decrease in agomir-29b-treated lungs (Figure 7B). Hydroxyproline assessment presented that silica induced an obvious increase in the lung, however, agomir-29b treatment blunted this effect (Figure 7C). Furthermore, silica instillation resulted in a significant increase in COL1A1 and FN (fibronectin gene) expression, which was also decreased with miR-29b treatment (Figure 6A).

In addition to using traditional methods to assess the progression of respiratory disease, we also evaluated the impact of silica and agomir-29b on lung function by the forced oscillation technique (FOT). The flexiVent FX system, including the basic model of total lung capacity (TLC), Snap Shot, Prime wave, and pressure-volume (PV) loop, was applied to measure the lung function of the mice. To evaluate the results objectively, the data from the mice in the silica, silica + NC, and silica + agomir-29b groups were compared to the reference value from the normal mice. Overall mechanics of the respiratory system were assessed using the Snap Shot module. Inspiratory capacity (IC), normalized to body weight, from the mice in the three groups appeared similar (Figure 8A). Silica increased elastic resistance (Ers) and respiratory resistance (Rrs) (Figures 8B and 8C) and significantly reduced respiratory system static compliance (Crs), as compared to the reference value (Figure 8D). Those of the silica + NC mice displayed a similar change to the silica mice, and agomir-29b weakened the change induced by silica.

The Prime wave module was further used to distinguish between airway resistance and lung resistance. Newtonian airway resistance (Rn [central airway resistance]) (Figure 8E) and the ratio of tissue damping and tissue elastance (G:H) (Figure 8H), from the mice in the silica group, were increased as compared to the corresponding

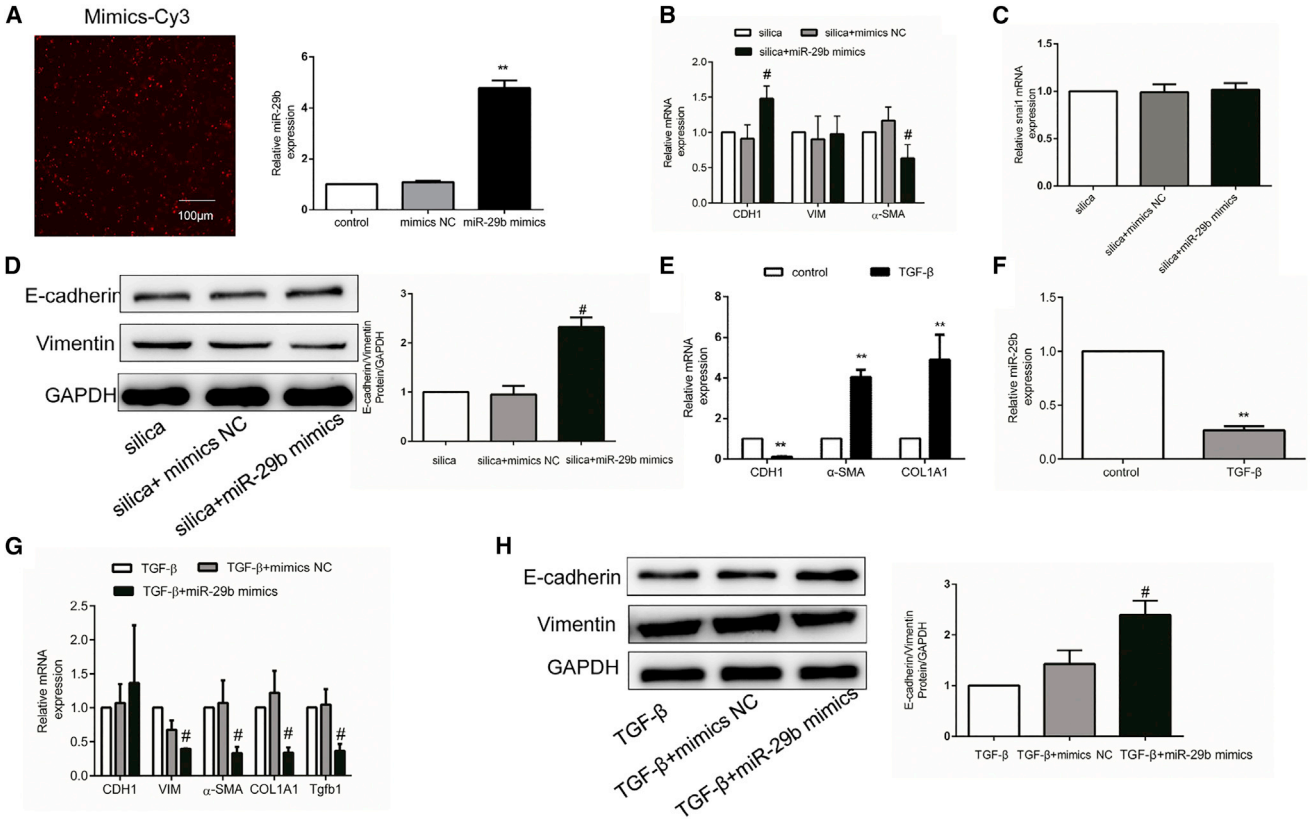

Figure 3. miR-29b Mimics Promoted MET and Reversed EMT in RLE-6TN Cells

After being incubated with silica (TGF-β1) for 24 hr, the RLE-6TN cells were incubated with silica (TGF-β1) in addition to miR-29b mimics or mimic negative control (NC) for an additional 24 hr. (A) The transfection efficiency was greater than 80% of the RLE-6TN cells transfected with Cy3-labeled miR-29b mimics, and qPCR analysis revealed that miR-29b mimics markedly increased the level of miR-29b in RLE-6TN cells. (B) qPCR analysis showed that miR-29b mimics increased the level of CDH1 and decreased the levels of VIM and α-SMA. (C) The results of qPCR suggested that miR-29b mimics did not alter the level of snai1. (D) Western blot analysis revealed that miR-29b mimics increased the ratio of E-cadherin:vimentin significantly in RLE-6TN cells. (E) TGF-β1 induced the downregulation of CDH1 expression and upregulation of VIM and α-SMA in RLE-6TN cells. (F) TGF-β1 induced the downregulation of miR-29b. (G) qPCR analysis showed that miR-29b mimics decreased the levels of VIM, α-SMA, COL1A1, and Tgfb1 compared with the TGF-β1 + mimic NC group. (H) Western blot analysis confirmed that miR-29b mimics increased the ratio of E-cadherin:vimentin significantly in the classical EMT model. All results were replicated at least three times independently. The data are presented as means ± SD. $^{*}p < 0.05$ and $^{**}p < 0.01$ versus the control group; $^{\#}p < 0.05$ and $^{\#\#}p < 0.01$ compared with the silica or TGF-β1 + mimic NC group.

reference value. In contrast, in the agomir-29b-treated mice, H was significantly increased compared with the silica and silica + NC mice (Figure 8G), resulting in a significantly decreased G:H compared to the silica and silica + NC mice (Figure 8H). Furthermore, these animals from the silica + agomir-29b group also showed a significant decrease in Rn in comparison to the silica + NC group (Figure 8E).

The PV loop model was specifically estimated by measurements of static compliance (Cst) and Salazar-Knowles equation parameters A and K (Figures 8I–8K). It was an effective and rapid way to differentiate fibrosis or other lung damages. The PV loops of mice in the silica group showed a characteristic downward shift, indicative of lung fibrosis, while that of agomir-29b mice displayed a typical upward shift, compared to the silica and silica + NC mice (Figure 8L). The area of the PV loop indicated that silica decreased the elastic recoil of the lung, while agomir-29b significantly increased the elastic recoil (Figure 8L). Consistent with IC, Cst from the silica group was unchanged compared to the reference value; however, Cst increased quite clearly in the silica + agomir-29b group as compared to the silica and silica + NC groups (Figure 8I). Overall, the analysis of respiratory mechanic parameters confirmed that silica resulted in damage to the respiratory function and agomir-29b could reduce the lung damage.

Taken together, these results suggested that, *in vivo*, miR-29b inhibited EMT, prevented lung fibrosis, and improved lung function, which was consistent with changes *in vitro*. Furthermore, miR-29b resulted in decreased pulmonary collagen and the expression of mesenchymal markers, but it increased the level of epithelial markers.

DISCUSSION

In the present study, we investigated the potential role of miRNAs in silicosis fibrosis. This study showed that a loss of miR-29b was

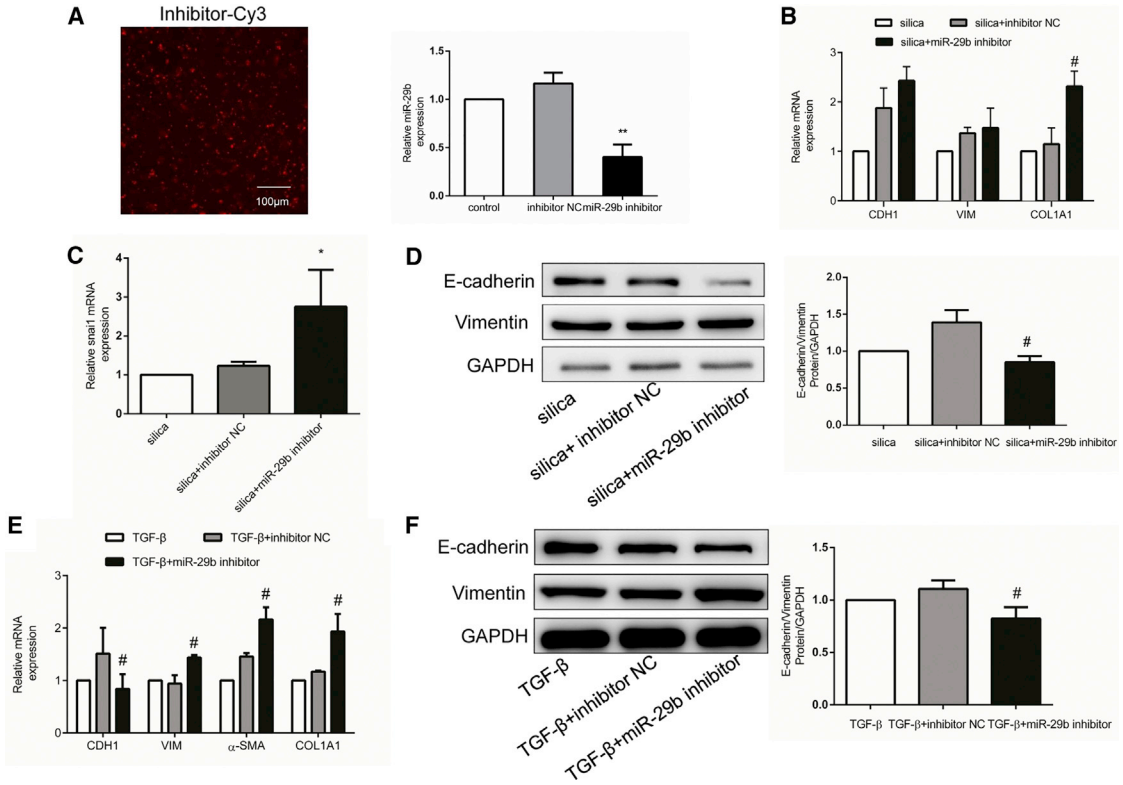

Figure 4. miR-29b Inhibitor Enhanced the Development of EMT in RLE-6TN Cells

After silica (TGF-β1) treatment for 24 hr, the RLE-6TN cells were incubated with silica (TGF-β1) plus miR-29b inhibitor or inhibitor NC for another 24 hr. (A) The transfection efficiency was greater than 80% of the RLE-6TN cells transfected with Cy3-labeled miR-29b inhibitor, and qPCR analysis revealed that miR-29b inhibitor markedly decreased the level of miR-29b in RLE-6TN cells. (B) qPCR analysis showed that miR-29b inhibitor increased the level of COL1A1 compared with the silica + inhibitor NC group but did not alter the levels of CDH1 and VIM. (C) qPCR for snai1 revealed similar results as with COL1A1. (D) miR-29b inhibitor decreased the ratio of E-cadherin:vimentin. (E) The results of qPCR showed that miR-29b inhibitor downregulated the expression of CDH1 but upregulated the expression of VIM, α-SMA, and COL1A1 in the TGF-β1 EMT model. (F) miR-29b inhibitor also decreased the ratio of E-cadherin:vimentin in the TGF-β1 EMT model. All results were replicated at least three times independently. The data are presented as means ± SD. $^{*}p < 0.05$ and $^{**}p < 0.01$ versus the control group; $^{\#}p < 0.05$ and $^{\#\#}p < 0.01$ compared with the silica or TGF-β1 inhibitor NC group.

associated with silica-induced EMT, pulmonary fibrosis, and respiratory function injury, whereas upregulation of miR-29b was capable of promoting MET, inhibiting EMT and lung fibrosis, as well as improving lung function. The findings suggested that miR-29b has therapeutic potential for silicosis fibrosis.

The miR-29 family is one of the most extensively studied miRNAs.[21] Previous studies have revealed that miR-29b is involved in a variety of diseases and pathophysiological processes, including embryonic development and tumor-related and fibrosis-related diseases.[22] Plaisier et al.[23] found that the miR-29 family inhibited specific genes associated with invasion and metastasis of lung adenocarcinoma. Montgomery et al.[24] found that therapeutic delivery of miR-29 mimics, during bleomycin-induced pulmonary fibrosis, reverses pulmonary fibrosis. Consistent with the above findings, this study has contributed new evidence regarding the protective role of miR-29b in silicosis fibrosis, especially its role in inducing MET and improving the pulmonary function.

It is well established that the injury of epithelial cells is vital in pulmonary fibrosis, and our previous findings sustained that EMT was involved in silicosis fibrosis. To establish a cell model of EMT, we stimulated RLE-6TN cells with silica or TGF-β1, which resulted in the increased expression of mesenchymal markers, decreased expression of epithelial markers, and a reduction in miR-29b simultaneously. Upregulation of miR-29b reversed the established EMT and induced MET, but the downregulation of miR-29b promoted EMT. *In vivo* silica induced EMT and the downregulation of miR-29b in the lung, however, agmiR-29b inhibited EMT. Interestingly, the key transcriptional factor Snail was not altered by miR-29b mimics or angomir-29b, but rather increased by miR-29b inhibitor. This indicated that the downregulation of miR-29b promoted EMT probably through increasing Snail, but the upregulation of miR-29b induced MET by a different target, which were consistent with the prior research.[25] One recent study identified that miR-29b could target the coding sequence of TGF-β1,[26] and some scholars found that miR-29b directly targeted the TGF-β signaling.[27] Hence, we

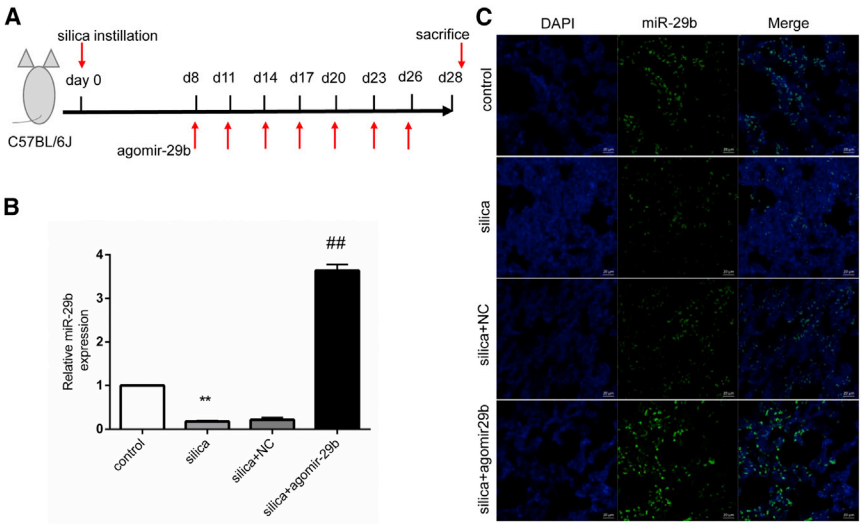

Figure 5. Agomir-29b Upregulated the Expression of miR-29b in the Lungs of Mice Instilled with Silica

(A) The experimental process of mice instilled with silica and following agomir-29b treatment. (B) Agomir-29b markedly increased the level of miR-29b in the lungs of the mice. (C) Representative FISH images showed that agomir-29b upregulated the expression of miR-29b in the lungs of mice instilled with silica. The data are presented as means ± SD (n = 6). $^{*}p < 0.05$ and $^{**}p < 0.01$ compared with the control group; $^{\#}p < 0.05$ and $^{\#\#}p < 0.01$ compared with the silica + NC group.

proposed that miR-29b may exert its MET effect by inhibiting TGF-β1 transcription. It is well known that TGF-β1 signaling plays a key role in TGF-β1-induced EMT, so we used TGF-β1 to stimulate RLE-6TN cells for 48 hr. We found that TGF-β1 downregulated miR-29b expression, whereas upregulation of miR-29b decreased the level of Tgfb1 and promoted MET, confirming the relationship between miR-29b and TGF-β1. Therefore, the data suggested that the blockade of TGF-β may be a potential mechanism by which upregulation of miR-29b promoted MET.

In this study, we also explored the potential mechanism whereby miR-29b inhibited silicosis fibrosis. First, promotion of MET and decreased TGF-β1 expression may contribute to the inhibitory effect of miR-29b on silicosis fibrosis. EMT contributed to silicosis fibrosis, while upregulation of miR-29b blunted EMT and promoted MET, resulting in fewer fibroblasts and less collagen production. TGF-β1 is known as the most powerful pro-fibrotic factor, and upregulation of miR-29b decreased the level of TGF-β1, resulting in fewer collagen matrices. Second, it is well known that miR-29b inhibits fibrogenesis by directly targeting mRNA 3′ UTRs of many collagen genes, including COL1A1 and so on.[28] In this study, we chose to test the COL1A1 level. Our results revealed that overexpression of miR-29b decreased silica-induced COL1A1 in RLE-6TN cells as well as in the lung exposed to silica. Conversely, miR-29b inhibitor increased COL1A1 expression. Therefore, miR-29b may repress the expression of basement membrane collagen matrix and inhibit lung fibrosis.

Inhibition of EMT and lung fibrosis may also be a mechanism by which miR-29b treatment improves lung function in a mouse model of silicosis. In this study, we performed lung function measurements with the objective of further assessing the lung function changes in silicosis mice and protective effects of miR-29b by FOT measurements. The measurements have already been used in mouse models of lung fibrosis diseases and proven to be particularly important in mouse models. In the present research, silica exposure decreased Crs and increased Ers and Rrs in the mice. In addition, Rn and G:H were upregulated, and the PV loop showed an obvious downward shift, which indicated that silica decreased the elastic recoil of the lung. This is in line with the earlier study of Devos et al.[29] However, IC and Cst in the silica group were almost unchanged compared to the normal mice, which suggested that the volume of the lung slightly altered at the early stage of silicosis; this is consistent with the phenomenon that silicosis may occur without symptoms. Agomir-29b is able to upregulate the Static compliance and G:H compared with the silica + NC group, which indicated that agomir-29b recovered the ability of lung parenchyma to stretch and expand. In addition, agomir-29b induced an upward shift in the PV loop, suggesting an upswing of elastic recoil. Meanwhile, agomir-29b also alleviated Rn, indicating agomir-29b had a therapeutic effect both in the peripheral and the central airways. Above all, the results of the lung function measurements confirmed that agomir-29b could blunt the lung impairment induced by silica.

In summary, we discovered that miR-29b, a miRNA significantly downregulated by silica, has the potential to promote MET, inhibit silicosis fibrosis, and improve lung function. The molecular mechanisms by which miR-29b exerted its function were probably determined by downregulation or upregulation of miR-29b. Furthermore, downregulation of miR-29b enhanced EMT, probably through upregulating the expression of snai1. Meanwhile, upregulation of miR-29b promoted MET by inhibiting TGF-β1, and it ultimately decreased collagen deposition by inhibiting COL1A1 level. The discovery may lead to the development of a new therapy that aims to postpone the process of this devastating disease.

MATERIALS AND METHODS

Silica Particle

Crystalline silica particles (Sigma, MO, USA), of which content was >99% and 95% of particle diameter was below 5 μm, were suspended in saline at a final concentration of 25 mg/mL for animal experiments and 2 mg/mL for cell experiments. The suspension of silica dust was sufficiently mixed by a vortex shaker. Penicillin (5,000 IU/mL) was transfused into the saline prior to instillation *in vivo*.

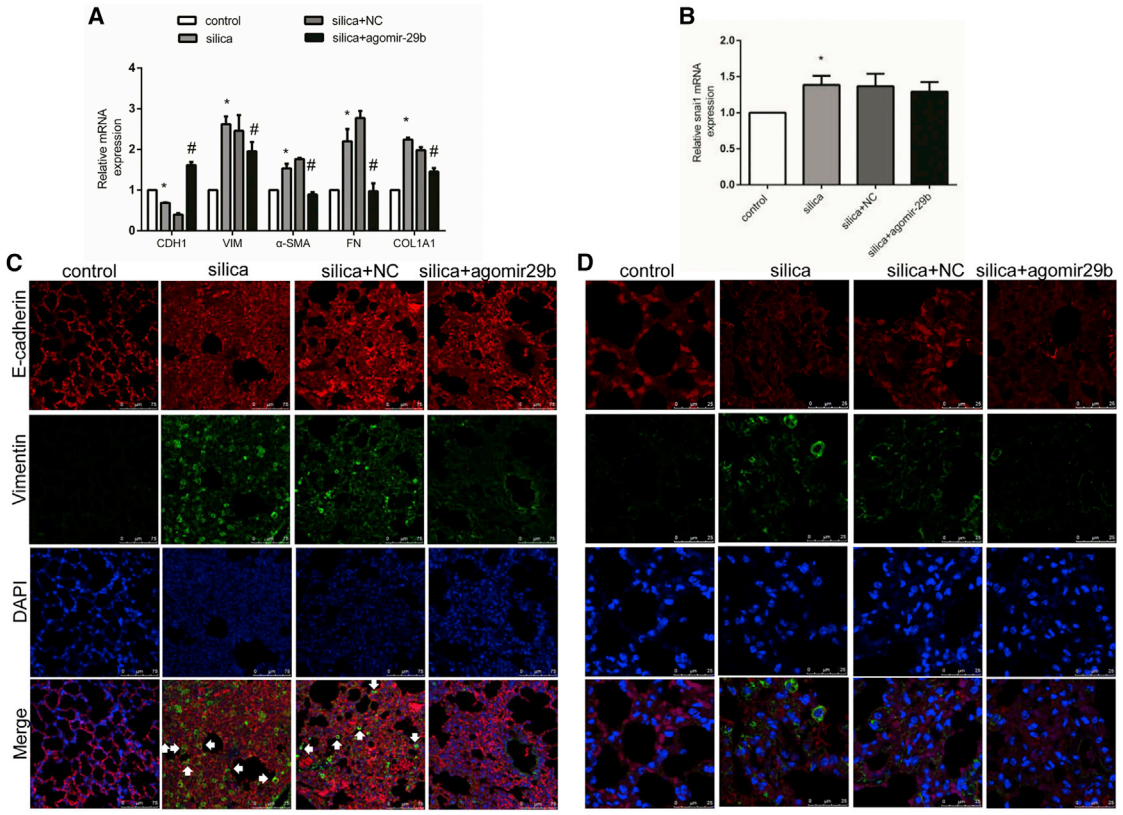

Figure 6. Agomir-29b Inhibited EMT and Decreased the Levels of ECM Genes in a Mouse Model of Silicosis Fibrosis

(A) The results of qPCR showed that agomir-29b upregulated the expression of CDH1 but downregulated the expression of VIM, α-SMA, and ECM genes (COL1A1 and FN). (B) Agomir-29b had no effect on the level of snai1. (C) Immunofluorescence staining suggested that the expression of vimentin was significantly increased following silica instillation but was decreased by agomir-29b treatment in alveolar epithelial cells (arrows), while the change of E-cadherin expression was not evident. (D) Amplified fluorescence images in the lungs of the mice. The data are presented as means ± SD (n = 6). $^{*}p < 0.05$ and $^{**}p < 0.01$ compared with the control group; $^{\#}p < 0.05$ and $^{\#\#}p < 0.01$ compared with the silica + NC group.

miRNA Microarray

Total RNA was extracted from A549 by using Trizol reagent, and then we tested miRNA microarray by using the Affymetrix Arrays (Gminix, Shanghai, China). The miRNA microarray analysis identified 38 miRNAs, and the TwoClassDif was used for data analysis; 3 miRNAs were identified to have at least a 1.5-fold change (p value <5%) in expression.

Mice and Ethics Statement

A total of 40 male C57BL/6J mice weighing 20–22 g was purchased from Vital River Laboratory Animal Technology (Beijing, China). Mice were housed in a temperature-controlled room (24°C ± 1°C) with a 12:12-hr light:dark cycle, and they were provided with sufficient food and water. This study was approved (AEEI-2017-017) by the Laboratory Animal Care and Use Committee at Capital Medical University.

Mouse Lung Fibrosis Model and Experimental Design

A total of 40 C57BL/6J mice was randomly divided into the control group (n = 10), silica group (n = 10), silica + NC group (n = 10), and silica + agomiR-29b group (n = 10). Mice were anesthetized with tribromoethanol 350 mg/kg (Sigma, St. Louis, MO, USA). Subsequently, mice were treated with intratracheal silica suspension 0.1 mL (2.5 mg), with the exception of mice in the control group, which received the same volume of saline instead. To investigate the effects of miR-29b *in vivo*, C57BL/6 mice were administered by caudal vein injection of the miR-29b agomiR (agomir-29b), at a dose of 5 nmol every 3 days (protocol summarized in Figure 5A). Moreover, delayed agomir-29b treatment was carried out on the eighth day when pulmonary fibrosis in the early stage was established (from eighth day after silica instillation). The mice in the control and silica groups were injected with an equal volume of saline, while silica + NC mice were administered agomir NC at a dose of 5 nmol. The mice were sacrificed on the 28th day. Four mice were used to assess lung function before sacrificing, and lung tissue sections were harvested for examination.

Cell Culture and Treatment

To select the optimum dose of silica in order to induce EMT and conduct microarray analysis, RAW264.7 (murine macrophage cell

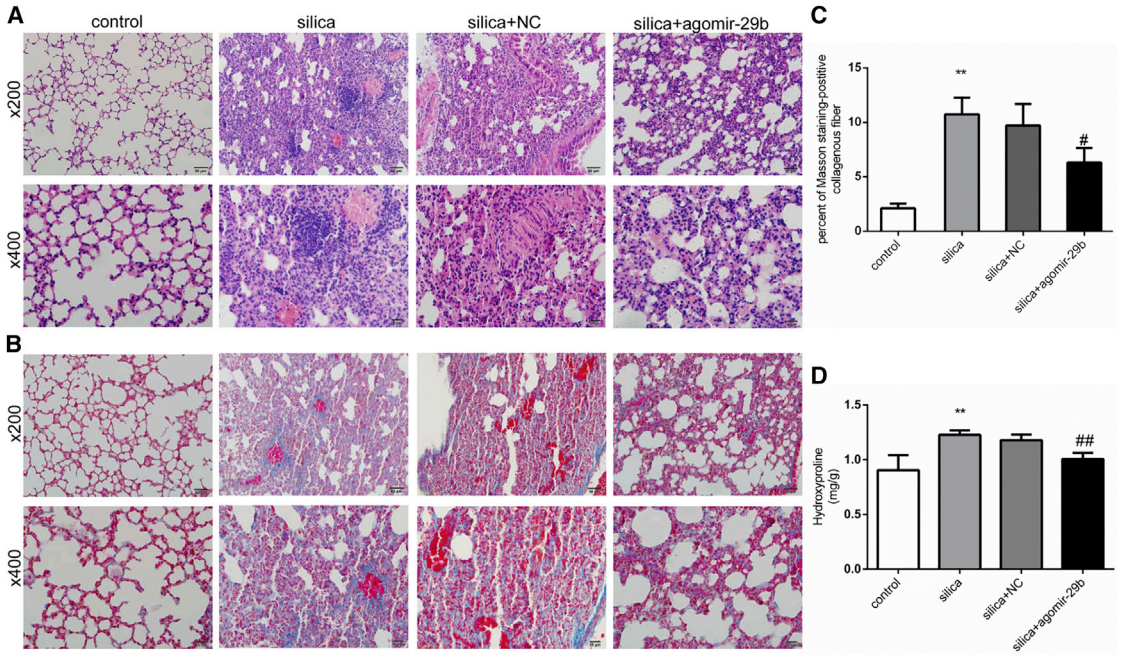

Figure 7. Agomir-29b Inhibited Pulmonary Fibrosis in Mice

(A) H&E staining in the lungs of the mice in each group at 28 days (light micrograph magnifications of 200× and 400×). (B) Masson staining in the lungs of the mice in each group at 28 days (light micrograph magnifications of 200× and 400×). (C) The percent of Masson staining-positive collagenous fiber was significantly increased in the silica group but decreased in the silica + agomir-29b group. (D) The content of HYP was significantly increased in the silica group but decreased in the silica + agomir-29b group. The data are presented as means ± SD (n = 6). $^{*}p < 0.05$ and $^{**}p < 0.01$ compared with the control group; $^{\#}p < 0.05$ and $^{\#\#}p < 0.01$ compared with the silica + NC group.

line) and A549 cells (human type II alveolar epithelial carcinoma cell line) were cultivated in DMEM added with 10% fetal bovine serum (FBS) (HyClone, Beijing, China) at 37°C with 5% CO_2 humidified. As soon as RAW264.7 cells were grown to 80% confluence, the cells were treated with different concentrations of silica (25, 50, and 100 μg/mL) for 24 hr. The supernatant was collected and subsequently treated as previously described.[30] A549 cells were maintained with the former silica supernatant for 48 hr and harvested for future experiments.

To observe the effect of silica on the morphology of RLE-6TN cells, RLE-6TN cells with multiple confluences (1×10^6, 5×10^5, and 2.5×10^5) were seeded in the 6-well plates. After the cells adhered to the plates, they were cultured with the supernatant of RAW264.7 cells stimulated by 50 μg/mL silica for 48 hr. Then the cells were photographed with a light microscope (Olympus D72, Japan).

To observe the effects of miR-29b mimics or inhibitor on EMT and MET, RAW264.7 and RLE-6TN cells (rat type II alveolar epithelial cell line) were grown in DMEM with 10% FBS (HyClone, Beijing, China) at 37°C with 5% CO_2 and 95% humidified air. The RLE-6TN cells were treated for 48 hr with either the supernatant of RAW264.7 cells stimulated by 50 μg/mL silica or 5 ng/mL recombinant human TGF-β1 (PeproTech, NJ, USA).

Wound-Healing Assay

The A549 cells were seeded into 6-well plates and cultured until 90% confluence. Then the surface of cells was scratched with a 200-μL pipette tip and washed twice using PBS. Subsequently, the cells were incubated with DMEM without or with the supernatant of RAW264.7 cells stimulated by 50 μg/mL silica. Photomicrographs were recorded at 0 and 24 hr.

miRNA Transfection

After silica treatment for 24 hr, RLE-6TN cells were transfected with 50 nM/L of either miR-29b mimics or mimic NC and 100 nM/L of either the miR-29b inhibitor or inhibitor NC (Sangong Biotech, Shanghai, China) using a transfection reagent (Lipofectamine RNAi MAX Reagent) in Opti-MEM Medium (Life Technologies, China), according to the manufacturer's instructions, for another 24 hr. miR-29b mimics and miR-29b inhibitor, with Cy3, were used to detect the transfection efficiency. The sequences used were synthetic as follows. The miR-29b mimic sense is 5′-UAGCACCAUUUGAAAUCAGUGUU-3′ and the antisense is 5′-CACUGAUUUCAAAUGGUGCUAUU-3′. The miR-29b inhibitor sense is 5′-AACACUGAUUUCAAAUGGUGCUA-3′.

RNA Isolation and Real-Time qPCR

Total RNA and miRNA were extracted from cells using TransZol Up (ET111, TransGen Biotech, Beijing, China), and mRNA was

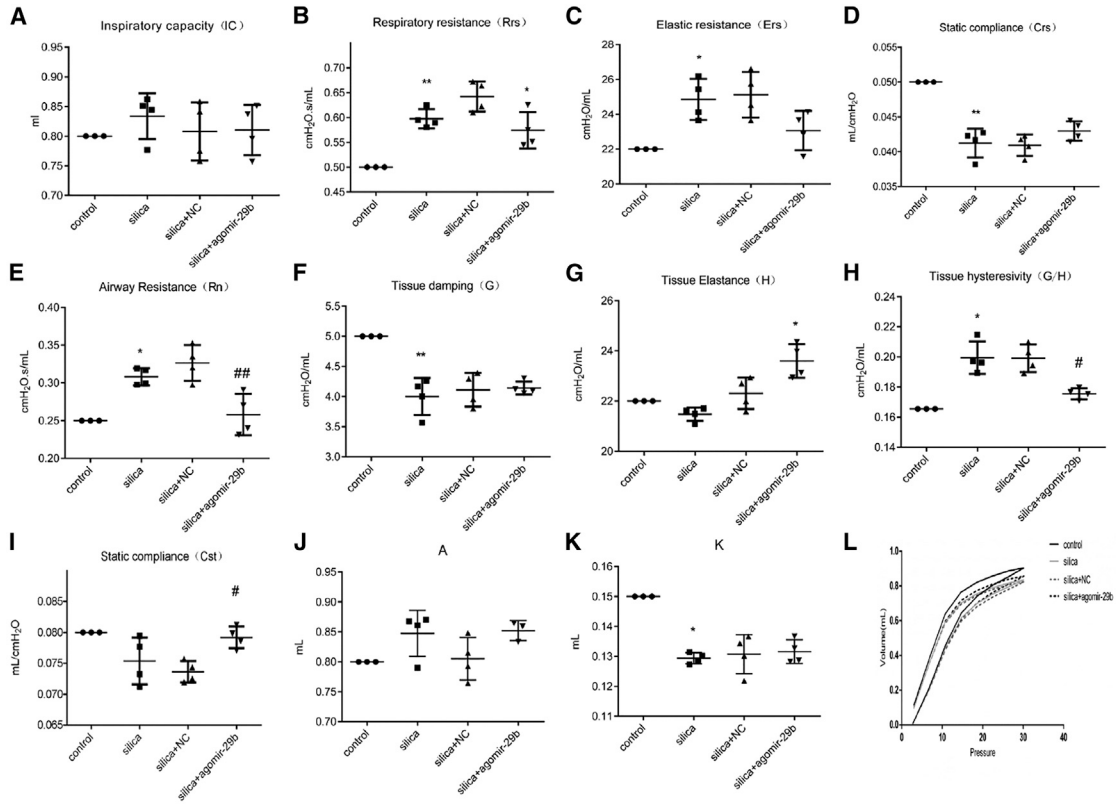

Figure 8. Agomir-29b Improved the Respiratory Function Damaged by Silica in the Mice

The flexiVent FX system was used to test the lung function, and results were compared with the reference value. The model of Snap Shot tested the inspiratory capacity (A), respiratory resistance (B), elastic resistance (C), and static compliance (D). The Prime wave measured airway resistance (E), tissue damping (F), tissue elastance (G), and tissue hysteresivity (H). PV loops were used to assess lung parenchyma static compliance (I), A (J), and K (K). The overall area of the PV loop revealed hysteresis (L). The data are presented as means ± SD (n = 4). $^{*}p < 0.05$ and $^{**}p < 0.01$ compared with the reference values; $^{\#}p < 0.05$ and $^{\#\#}p < 0.01$ compared with the silica + NC group.

transcribed to cDNA using the TransScript First-Strand cDNA Synthesis SuperMix (AT301, TransGen Biotech, Beijing, China). The cDNA of miRNA was utilized for the TransScript miRNA First-Strand cDNA Synthesis SuperMix (AT351, TransGen Biotech, Beijing, China). qPCR was performed with the CFX96 real-time qPCR detection system (Bio-Rad, Hercules, CA), using the SYBR Green qPCR kit (AQ141, TransGen Biotech, Beijing, China). The level of gene expression was calculated by normalizing to glyceraldehyde-3-phosphate dehydrogenase using the $2^{-\Delta\Delta CT}$ method. The primer sequences used are given in Table S1.

Western Blot

Protein extracts were performed with Kit KGP2100 (KeyGen Biotech, China) according to the manufacturer's instructions. The collected cells were treated three times with 4°C PBS and disrupted sufficiently in the lysis buffer. The concentration of the protein was measured by using bicinchoninic acid (BCA, Thermo Scientific, Rockford, IL, USA). Equal amounts of protein (20 μg) were separated in 10% SDS polyacrylamide gels and transferred onto polyvinylidene fluoride (PVDF) membranes (Millipore, Billerica, MA, USA). Subsequently, it was blocked in 5% BSA solution and incubated overnight at 4°C with primary antibodies against E-cadherin (1:1,000; Abcam, CA, USA), vimentin (1:1,000; Abcam, CA, USA), collagen I (1:5,000; Abcam, CA, USA), Snail (1:1,000; Cell Signaling Technology, Boston, MA, USA), or GAPDH (1:1,000; Cell Signaling Technology, Boston, MA, USA). Anti-rabbit immunoglobulin G (IgG), horseradish peroxidase (HRP)-linked antibody (1:2,000; Cell Signaling Technology, Boston, MA, USA), and Anti-mouse IgG, HRP-linked antibody (1:2,000; Cell Signaling Technology, Boston, MA, USA) were used as the secondary antibodies. The stripe of protein was detected with enhanced chemiluminescence method (ECL, Thermo Fisher Scientific) and captured by Tanon-5200 system (Beijing Yuan Ping Hao Biotech). The quantification was calculated by ImageJ software to analyze the intensity of the gray scale images.

MTT Assay

MTT assay was used to test the cell viability of A549 cells. The cells were treated with different concentrations of silica (25, 50, and 100 μg/mL) and incubated at 37°C in 5% (v/v) CO_2 for up to 48 hr, and then they

were incubated with MTT for 4 hr and a DMSO solution later. The absorbance was measured at 490 nm.

FISH

FISH was conducted with the paraffin-embedded lung tissue according to a protocol described previously.[31] Briefly, after deparaffinized and rehydrated, the slides were incubated with 20 μg/mL proteinase K for 10 min at 37 °C, and then they were hybridized with the probe specific to miR-29b overnight. The anti-biotin-labeled fluorescein isothiocyanate was applied to visualize the positive signals. Then the images were captured using fluorescence microscopy. The sequence of miR-29b in mice is given in Table S1.

Hydroxyproline Analysis

Lung hydroxyproline was analyzed with a hydroxyproline colorimetric assay kit from Nanjing Jiancheng biotechnology research institution (Nanjing, China), following the manufacturer's instructions. The hydroxyproline concentrations were expressed as milligrams per gram protein.

H&E and Masson Staining

The right lungs of the mice were removed and fixed in 10% formalin for 48 hr. After which, they were embedded in paraffin and cut into 5-mm-thick slices. The lung tissue sections were observed with the light microscope (Olympus D72, Japan) with 200× magnifications.

Immunofluorescence

Immunofluorescence *in vitro* was performed as we previously described. Immunofluorescence *in vivo* was as follows: paraffin-embedded lung tissue was treated with deparaffinization, rehydration, and antigen retrieval. After being washed by PBS, it was fixed with 0.1% Triton X-100 for 20 min. After being rinsed in PBS and blocked with 3% BSA for 10 min, slides were incubated with primary antibodies against E-cadherin (1:100; Abcam, CA, USA) or vimentin (1:100; Abcam, CA, USA) overnight at 4°C. After being washed by PBS 3 times, slides were incubated with the secondary antibodies conjugated to fluorescein isothiocyanate (FITC) for 1 hr at room temperature (RT). At this point, they were rinsed again and counterstained with DAPI. The images were captured with laser-scanning confocal fluorescence microscopy.

Lung Function Measurements

The data relating to respiratory function were collected from the flexiVent FX system (SCIREQ, Montreal, QC, Canada), equipped with an FX module and operated by the flexiVent version (v.)7.6 software. Mice were anesthetized with pentobarbital (100 mg/kg) (CEVA, Brussels, Belgium) by intraperitoneal injection. Then, the trachea was exposed so that we were able to insert a metal cannula, which was connected to the tubing system extended from the machine. Following the rhythm of spontaneous breathing, the apparatus ventilated the mice quasi-sinusoidally with a tidal volume of 10 mL/kg at a frequency of 150 breaths/min and a positive end-expiratory pressure of 2 cmH_2O. The lung function measurements were made by automatic operation. Briefly, IC was measured by lung inflations to 30 cmH_2O over 3 s. Measured values of overall respiratory system resistance (Rrs), compliance (Crs), and elastance (Ers) were obtained from single-frequency forced oscillation maneuvers. The model of Prime wave maneuver was utilized to calculate respiratory input impedance. The multiple prime frequencies ranged from 0.25 to 20 Hz. The parameters of Rn, G, and H were analyzed, and the coefficient of determination was ≥ 0.95. PV curves were collected and the data of stepwise increases and decreases airway pressure subsequently. Cst was calculated from the slope of each curve. The area (hysteresis) of the PV curve as well as the shape parameter (A or K) describing the deflation limb of the PV loop were also calculated.

Statistical Analysis

Data are presented as the mean ± SD. Multiple comparisons were used for the calculation of one-way ANOVA followed by the Student-Newman-Keuls post hoc test. All statistical analyses were performed by SPSS 22.0 software (SPSS, Chicago, IL, USA). The p value less than 0.05 was considered statistically significant. All results were replicated at least three times independently.

Accession Numbers

We have uploaded the raw data to Mendeley: https://doi.org/10.17632/dx86xxknr4.1.

SUPPLEMENTAL INFORMATION

Supplemental Information includes one figure and one table and can be found with this article online at https://doi.org/10.1016/j.omtn.2018.10.017.

AUTHOR CONTRIBUTIONS

L.T., Y.W., and Z.Z. designed and supervised the study. J.S., Q.L., and W.P. performed the mouse experiments and analyzed the data. J.S., X.L., and X.C. performed the cell experiments and analyzed the data. Y.W. and J.S. analyzed the data and wrote the manuscript. A.A. edited the manuscript. All authors read and approved the final version of the manuscript.

CONFLICTS OF INTEREST

The authors declare no competing interests.

ACKNOWLEDGMENTS

This work was supported by grants of National Natural Science Foundation of China (81273047, 91643114, 81472958, 81703197, and 81602832) and Key Projects of Science and Technology Program by Beijing Municipal Education Commission (KZ201610025020).

REFERENCES

1. Cohen, R.A., Petsonk, E.L., Rose, C., Young, B., Regier, M., Najmuddin, A., Abraham, J.L., Churg, A., and Green, F.H. (2016). Lung Pathology in U.S. Coal Workers with Rapidly Progressive Pneumoconiosis Implicates Silica and Silicates. Am. J. Respir. Crit. Care Med. *193*, 673–680.

2. Leung, C.C., Yu, I.T., and Chen, W. (2012). Silicosis. Lancet *379*, 2008–2018.

3. Richeldi, L., Collard, H.R., and Jones, M.G. (2017). Idiopathic pulmonary fibrosis. Lancet *389*, 1941–1952.

4. Li, L.F., Chu, P.H., Hung, C.Y., Kao, W.W., Lin, M.C., Liu, Y.Y., and Yang, C.T. (2013). Lumican regulates ventilation-induced epithelial-mesenchymal transition through extracelluar signal-regulated kinase pathway. Chest *143*, 1252–1260.

5. Li, L.F., Kao, K.C., Liu, Y.Y., Lin, C.W., Chen, N.H., Lee, C.S., Wang, C.W., and Yang, C.T. (2017). Nintedanib reduces ventilation-augmented bleomycin-induced epithelial-mesenchymal transition and lung fibrosis through suppression of the Src pathway. J. Cell. Mol. Med. *21*, 2937–2949.

6. van Meeteren, L.A., and ten Dijke, P. (2012). Regulation of endothelial cell plasticity by TGF-β. Cell Tissue Res. *347*, 177–186.

7. Yang, G., Zhu, Z., Wang, Y., Gao, A., Niu, P., and Tian, L. (2013). Bone morphogenetic protein-7 inhibits silica-induced pulmonary fibrosis in rats. Toxicol. Lett. *220*, 103–108.

8. Liang, D., Wang, Y., Zhu, Z., Yang, G., An, G., Li, X., Niu, P., Chen, L., and Tian, L. (2016). BMP-7 attenuated silica-induced pulmonary fibrosis through modulation of the balance between TGF-β/Smad and BMP-7/Smad signaling pathway. Chem. Biol. Interact. *243*, 72–81.

9. Esteban, M.A., Bao, X., Zhuang, Q., Zhou, T., Qin, B., and Pei, D. (2012). The mesenchymal-to-epithelial transition in somatic cell reprogramming. Curr. Opin. Genet. Dev. *22*, 423–428.

10. Thiery, J.P., and Sleeman, J.P. (2006). Complex networks orchestrate epithelial-mesenchymal transitions. Nat. Rev. Mol. Cell Biol. *7*, 131–142.

11. Zhang, J., and Ma, L. (2012). MicroRNA control of epithelial-mesenchymal transition and metastasis. Cancer Metastasis Rev. *31*, 653–662.

12. Lamouille, S., Xu, J., and Derynck, R. (2014). Molecular mechanisms of epithelial-mesenchymal transition. Nat. Rev. Mol. Cell Biol. *15*, 178–196.

13. Pandit, K.V., Corcoran, D., Yousef, H., Yarlagadda, M., Tzouvelekis, A., Gibson, K.F., Konishi, K., Yousem, S.A., Singh, M., Handley, D., et al. (2010). Inhibition and role of let-7d in idiopathic pulmonary fibrosis. Am. J. Respir. Crit. Care Med. *182*, 220–229.

14. Belgardt, B.F., Ahmed, K., Spranger, M., Latreille, M., Denzler, R., Kondratiuk, N., von Meyenn, F., Villena, F.N., Herrmanns, K., Bosco, D., et al. (2015). The microRNA-200 family regulates pancreatic beta cell survival in type 2 diabetes. Nat. Med. *21*, 619–627.

15. Wang, Y., Liang, D., Zhu, Z., Li, X., An, G., Niu, P., Chen, L., and Tian, L. (2016). Bone morphogenetic protein-7 prevented epithelial-mesenchymal transition in RLE-6TN cells. Toxicol. Res. (Camb.) *5*, 931–937.

16. Yan, W., Xiaoli, L., Guoliang, A., Zhonghui, Z., Di, L., Ximeng, L., Piye, N., Li, C., and Lin, T. (2016). SB203580 inhibits epithelial-mesenchymal transition and pulmonary fibrosis in a rat silicosis model. Toxicol. Lett. *259*, 28–34.

17. Das, S., Kumar, M., Negi, V., Pattnaik, B., Prakash, Y.S., Agrawal, A., and Ghosh, B. (2014). MicroRNA-326 regulates profibrotic functions of transforming growth factor-β in pulmonary fibrosis. Am. J. Respir. Cell Mol. Biol. *50*, 882–892.

18. Eulalio, A., Mano, M., Dal Ferro, M., Zentilin, L., Sinagra, G., Zacchigna, S., and Giacca, M. (2012). Functional screening identifies miRNAs inducing cardiac regeneration. Nature *492*, 376–381.

19. Lian, X., Chen, X., Sun, J., An, G., Li, X., Wang, Y., Niu, P., Zhu, Z., and Tian, L. (2017). MicroRNA-29b inhibits supernatants from silica-treated macrophages from inducing extracellular matrix synthesis in lung fibroblasts. Toxicol. Res. (Camb.) *6*, 878–888.

20. Cushing, L., Kuang, P.P., Qian, J., Shao, F., Wu, J., Little, F., Thannickal, V.J., Cardoso, W.V., and Lü, J. (2011). miR-29 is a major regulator of genes associated with pulmonary fibrosis. Am. J. Respir. Cell Mol. Biol. *45*, 287–294.

21. Maurer, B., Stanczyk, J., Jüngel, A., Akhmetshina, A., Trenkmann, M., Brock, M., Kowal-Bielecka, O., Gay, R.E., Michel, B.A., Distler, J.H., et al. (2010). MicroRNA-29, a key regulator of collagen expression in systemic sclerosis. Arthritis Rheum. *62*, 1733–1743.

22. Ślusarz, A., and Pulakat, L. (2015). The two faces of miR-29. J. Cardiovasc. Med. (Hagerstown) *16*, 480–490.

23. Plaisier, C.L., Pan, M., and Baliga, N.S. (2012). A miRNA-regulatory network explains how dysregulated miRNAs perturb oncogenic processes across diverse cancers. Genome Res. *22*, 2302–2314.

24. Montgomery, R.L., Yu, G., Latimer, P.A., Stack, C., Robinson, K., Dalby, C.M., Kaminski, N., and van Rooij, E. (2014). MicroRNA mimicry blocks pulmonary fibrosis. EMBO Mol. Med. *6*, 1347–1356.

25. Pattabiraman, D.R., Bierie, B., Kober, K.I., Thiru, P., Krall, J.A., Zill, C., Reinhardt, F., Tam, W.L., and Weinberg, R.A. (2016). Activation of PKA leads to mesenchymal-to-epithelial transition and loss of tumor-initiating ability. Science *351*, aad3680.

26. Zhang, Y., Huang, X.R., Wei, L.H., Chung, A.C., Yu, C.M., and Lan, H.Y. (2014). miR-29b as a therapeutic agent for angiotensin II-induced cardiac fibrosis by targeting TGF-β/Smad3 signaling. Mol. Ther. *22*, 974–985.

27. Xiao, J., Meng, X.M., Huang, X.R., Chung, A.C., Feng, Y.L., Hui, D.S., Yu, C.M., Sung, J.J., and Lan, H.Y. (2012). miR-29 inhibits bleomycin-induced pulmonary fibrosis in mice. Mol. Ther. *20*, 1251–1260.

28. He, Y., Huang, C., Lin, X., and Li, J. (2013). MicroRNA-29 family, a crucial therapeutic target for fibrosis diseases. Biochimie *95*, 1355–1359.

29. Devos, F.C., Maaske, A., Robichaud, A., Pollaris, L., Seys, S., Lopez, C.A., Verbeken, E., Tenbusch, M., Lories, R., Nemery, B., et al. (2017). Forced expiration measurements in mouse models of obstructive and restrictive lung diseases. Respir. Res. *18*, 123.

30. Wang, Y., Yang, G., Zhu, Z., Liang, D., Niu, P., Gao, A., Chen, L., and Tian, L. (2015). Effect of bone morphogenic protein-7 on the expression of epithelial-mesenchymal transition markers in silicosis model. Exp. Mol. Pathol. *98*, 393–402.

31. Pena, J.T., Sohn-Lee, C., Rouhanifard, S.H., Ludwig, J., Hafner, M., Mihailovic, A., Lim, C., Holoch, D., Berninger, P., Zavolan, M., and Tuschl, T. (2009). miRNA in situ hybridization in formaldehyde and EDC-fixed tissues. Nat. Methods *6*, 139–141.

OMTN, Volume *14*

Supplemental Information

MicroRNA-29b Mediates Lung Mesenchymal-Epithelial Transition and Prevents Lung Fibrosis in the Silicosis Model

Jingping Sun, Qiuyue Li, Ximeng Lian, Zhonghui Zhu, Xiaowei Chen, Wanying Pei, Siling Li, Ali Abbas, Yan Wang, and Lin Tian

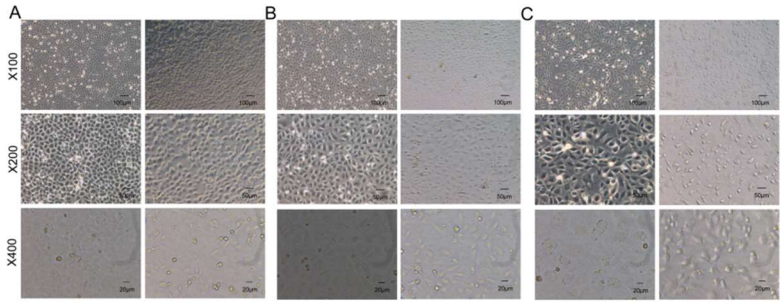

Figure S1

Figure S1. Silica induced the morphology change of RLE-6TN cells.

Exposure with silica for 48h induced a spindle-shaped change in RLE-6TN cells regardless of high (Figure S1A), medium (Figure S1B) and low (Figure S1C) confluence.

Table S1. The primer sequences of mRNA and miRNA

Oligo	Species	Forward Sequences 5'-3'	Reverse Sequences 3'-5'
GAPDH	Mouse	AAGAAGGTGGTGAAGCAGGC	TCCACCACCCTGTTGCTGTA
CDH1	Mouse	GATCCTGAGCTGCCTCACAA	CAGCCTGAACCACCAGAGTG
VIM	Mouse	CTGAGGCTGCCAACCGGAACAA	CCTCGCCTTCCAGCAGCTTCC
α-SMA	Mouse	GAGCATCCGACACTGCTGAC	GCACAGCCTGAATAGCCA CA
COL1A1	Mouse	GCTCCTCTTAGGGGCCACT	CCACGTCTCACCATTGGGG
FN	Mouse	CATTCCTGTGGGGATGGATTC	TACGTGCAAGCACACCGATTT
Snai1	Mouse	TAGAGCTGACCTCGCTGTCC	GAGGTGGACGAGAAGGACGA
GAPDH	Rat	AAGAAGGTGGTGAAGCAGGC	TCCACCACCCTGTTGCTGTA
CDH1	Rat	ATGAGGTCGGTGCCCGTATT	CTCGTTGGTCTTGGGGTCTGT
VIM	Rat	CTGCTGGAAGGGGAGGAGAG	GGTCATCGTGGTGCTGAGAAG
α-SMA	Rat	CACGGCATCATCACCAACTG	CCACGCGAAGCTCGTTATAGA
COL1A1	Rat	CAATGGCACGGCTGTGTGCG	CACTCGCCCTCCCGTCTTTGG
Snai1	Rat	AGAAGCCTTTCTCCTGCTCC	CACTGGTATCTCTTCACATCCGA
Tgfb1	Rat	CGCAACAACGCAATCTATG	ACCAAGGTAACGCCAGGA
U6	Human mouse rat	GACACGCAAATTCGTGAAGC	
miR-29b-3p	Human mouse rat	UAGCACCAUUUGAAAUCAGUGUU	